[F-18]MEL050 as a melanin-targeted PET tracer: fully automated radiosynthesis and comparison to F-18-FDG for the detection of pigmented melanoma in mice primary subcutaneous tumors and pulmonary metastases

Rizzo-Padoin, N.; Chaussard, M.; Vignal, N.; Kotula, E.; Tsoupko-Sitnikov, V.; Vaz, S.; ... ; Sarda-Mantel, L.

Nuclear Medicine and Biology 43 (2016) 773–780

Contents lists available at ScienceDirect

Nuclear Medicine and Biology

journal homepage: www.elsevier.com/locate/nucmedbio

[^{18}F]MEL050 as a melanin-targeted PET tracer: Fully automated radiosynthesis and comparison to ^{18}F-FDG for the detection of pigmented melanoma in mice primary subcutaneous tumors and pulmonary metastases

Nathalie Rizzo-Padoin [a,b,*], Michael Chaussard [a], Nicolas Vignal [a,b], Ewa Kotula [c], Vadim Tsoupko-Sitnikov [a], Sofia Vaz [d], Fortune Hontonnou [a,e], Wang-Qing Liu [f], Jean-Luc Poyet [c,e], Michel Vidal [f], Pascal Merlet [e,g], Benoit Hosten [a,b], Laure Sarda-Mantel [a,d,e,h]

[a] Assistance Publique – Hôpitaux de Paris, Hôpital Saint-Louis, Unité Claude Kellershohn, Paris, 75010, France
[b] Inserm, UMR-S 1144, Faculté de Pharmacie de Paris, Université Paris Descartes, Paris, 75006, France
[c] Inserm, UMRS 1160, Institut Universitaire d'Hématologie, Hôpital Saint-Louis, Paris, 75010, France
[d] Assistance Publique – Hôpitaux de Paris, Hôpital Lariboisière, Médecine nucléaire, Paris, 75010, France
[e] Université Paris Diderot, Paris, 75010, France
[f] UMR 8638 CNRS, Faculté de Pharmacie de Paris, Université Paris Descartes, Paris, 75006, France
[g] Assistance Publique – Hôpitaux de Paris, Hôpital Saint-Louis, Médecine nucléaire, Paris, 75010, France
[h] Inserm UMR-S 942, Hôpital Lariboisière, Paris, 75010, France

ARTICLE INFO

Article history:
Received 14 June 2016
Received in revised form 9 August 2016
Accepted 16 August 2016

Keywords:
PET imaging
[^{18}F]MEL050
Melanoma
Melanin
Small-animal PET
Radiosynthesis

ABSTRACT

Introduction: Melanoma is a highly malignant cutaneous tumor of melanin-producing cells. MEL050 is a synthetic benzamide-derived molecule that specifically binds to melanin with high affinity. Our aim was to implement a fully automated radiosynthesis of [^{18}F]MEL050, using for the first time, the AllInOne™ synthesis module (Trasis), and to evaluate the potential of [^{18}F]MEL050 for the detection of pigmented melanoma in mice primary subcutaneous tumors and pulmonary metastases, and to compare it with that of [^{18}F]FDG.
Methods: Automated radiosynthesis of [^{18}F]MEL050, including HPLC purification and formulation, were performed on an AllInOne™ synthesis module. [^{18}F]MEL050 was synthesized using a one-step bromine-for-fluorine nucleophilic heteroaromatic substitution.
Melanoma models were induced by subcutaneous (primary tumor) or intravenous (pulmonary metastases) injection of B16-F10-luc2 cells in NMRI mice. The maximum percentage of [^{18}F]MEL050 Injected Dose per g of lung tissue (%ID/g Max) was determined on PET images, compared to [^{18}F]FDG and correlated to *in vivo* bioluminescence imaging.
Results: The automated radiosynthesis of [^{18}F]MEL050 required an overall radiosynthesis time of 48 min, with a yield of 13–18% (not-decay corrected) and radiochemical purity higher than 99%. [^{18}F]MEL050 PET/CT images were concordant with bioluminescence imaging, showing increased radiotracer uptake in all primary subcutaneous tumors and pulmonary metastases of mice. PET quantification of radiotracers uptake in tumors and muscles demonstrated similar tumor-to-background ratio (TBR) with [^{18}F]MEL050 and [^{18}F]FDG in subcutaneous tumors and higher TBR with [^{18}F]MEL050 than with [^{18}F]FDG in pulmonary metastases.
Conclusion: We successfully implemented the radiosynthesis of [^{18}F]MEL050 using the AllInOne™ module, including HPLC purification and formulation. *In vivo* PET/CT validation of [^{18}F]MEL050 was obtained in mouse models of pigmented melanoma, where higher [^{18}F]MEL050 uptake was observed in sub-millimetric pulmonary metastases, comparatively to [^{18}F]FDG.

1. Introduction

Melanoma is a highly malignant tumor of pigment-producing cells (melanocytes). It is the most severe type of skin cancer, with a high potential for metastatic spread. Even if melanoma accounts for only 4% of all skin cancers, it causes the greatest number of skin cancer-related deaths worldwide. Early detection of thin cutaneous melanoma is the best way to reduce mortality [1].

* Corresponding author at: Hôpital Saint-Louis, Unité Claude Kellershohn, bâtiment Hayem, 1 Avenue Claude Vellefaux, 75010, Paris, France. Tel.: +33 1 42 38 51 05; fax: +33 1 42 49 45 97.
E-mail address: nathalie.rizzo@aphp.fr (N. Rizzo-Padoin).

http://dx.doi.org/10.1016/j.nucmedbio.2016.08.010
0969-8051/

The incidence rate of melanoma has more than tripled in the white population during the last 30 years and it continues to rise worldwide. In 2016, it is estimated that there will be 76,380 new cases of melanoma of the skin and an estimated 10,130 people will die of this disease in the United States [2]. The ongoing trend of rising melanoma incidence rates in most white populations is projected to continue over the next two to three decades. Even though mortality rates have stabilized in several countries, as a result of earlier detection and screening, the incidence of thick potentially fatal melanomas remains constant, and is perhaps even increasing [3]. In France, cutaneous melanoma is the 11th most common cancer in both sexes, with an estimation of 14,325 new cases in 2015 [4].

Although early detection, appropriate surgery, and adjuvant therapy have improved outcomes, the prognosis of metastatic melanoma remains very poor. Advanced melanoma is still associated with an extremely poor median survival, ranging from 2 to 8 months, with only 5% surviving more than 5 years and remains one of the most treatment-refractory malignancies. Many agents have been investigated for antitumor activity in melanoma but the current treatment options for patients with metastatic disease are limited and non-curative in the majority of cases [5,6]. Conventional treatments for melanoma, including chemotherapy, radiation therapy or immunotherapy are associated with low progression-free survival rates and impaired by significant adverse effects [7,8]. The 3-year survival rate is less than 15% [9]. Survival largely depends on the stage of detection [10]. The patient's outcome is highly dependent on the early detection of metastasis and on the accuracy of staging. Powerful tools for both early detection and evaluation of new efficient treatment strategies of melanoma are therefore urgently needed.

[^{18}F]FDG Positron Emission Tomography (PET) imaging is routinely used for initial staging of III/IV malignant melanoma (detection of distant metastases), and seems to be useful for therapeutic follow-up [11]. It is not sensitive enough for the detection of local and lymph node metastases in stage I/II melanomas.

Besides [^{18}F]FDG, radiolabelled benzamide (BZ) derivatives appear as interesting compounds for sensitive detection of pigmented malignant melanomas. They exhibit high and specific binding with melanin in melanoma cells and melanocytes [12,13]. Promising results were obtained with these benzamide derivatives for both diagnosis and therapeutic applications [14,15]. Clinical trials have shown the usefulness of ^{123}I-BZA and ^{123}I-BZA2 for detection of melanoma and its metastases with high specificity and sensitivity [16–18].

MEL050 is one of the synthetic benzamide derived molecules that specifically binds to melanin with high affinity. It was used as a PET tracer for pigmented melanoma after radiolabelling with F-18 in experimental models [19,20]. Nevertheless, the automated radiosynthesis of [^{18}F]MEL050 was invested in by only few authors and the product potential has been studied in few preclinical and clinical studies. Therefore, we report here our efforts to develop an appropriate radiosynthesis of [^{18}F]MEL050 using a new radiosynthesis module AllInOne that has recently become available. Our aim was to implement a fully automated radiosynthesis of [^{18}F]MEL050, including HPLC purification and formulation, using for the first time, the AllInOne™ radiosynthesis platform. For this purpose, we also implemented purification and formulation processes on this new radiosynthesis platform. In order to validate *in vivo* the radiotracer we produced, PET/CT imaging was performed in control mice and in mice models of pigmented melanoma, primary subcutaneous tumors and pulmonary metastases, and we also compared [^{18}F] MEL050 and [^{18}F]FDG PET imaging in these mice models.

2. Materials and methods

2.1. Radiochemical synthesis of [^{18}F]MEL050

2.1.1. General

All reagents and solvents were purchased from commercial suppliers (ABX or Sigma-Aldrich) and were used without further purification. Sep.-Pak QMA and C18 were purchased respectively from ABX and Waters. [^{18}F]fluoride was produced *via* the [^{18}O(p,n)^{18}F] nuclear reaction (IBA Cyclone 18/9 cyclotron). The bromo-precursor, N-[2-(Diethylamino)ethyl]-6-bromonicotinamide, and the standard N-[2- (diethylamino)ethyl]-6-fluoronicotinamide (MEL050) were synthesized according to published procedure [21].

Automated radiosynthesis, HPLC purification and formulation of [^{18}F] MEL050 were performed on an AllInOne™ synthesis module (Trasis, Ans, Belgium). Semi-preparative HPLC purification was conducted on a Waters Symmetry® Semi-Prep C18 column (300 × 7.8 mm, 7 μm) using isocratic elution conditions with acetonitrile/20 mM ammonium bicarbonate [NH_4HCO_3] (20:80, *v*/v) as mobile phase at a flow rate of 3.0 mL/min.

The presence of acetonitrile in the preparative HPLC mobile phase, incompatible with *in vivo* experimentation, required introduction of formulation after the purification step. This was implemented according to the classical dilution – fixation – elution scheme using a C18 cartridge.

Radioactivity of the final product was measured with a dose calibrator (PET DOSE 5 Ci, COMECER).

Analytical HPLCs were performed on a Dionex Ultimate 3000 (Thermofisher Scientific) with a multi-wavelength UV Diode Array Detector (DAD) in series with a Bioscan gamma detector (Camberra, St Quentin Yvelines, France) using a Waters Symmetry® C18 column (150 × 4.6 mm, 5 μm). A delay time of 20 s was observed between the two detectors. The gradient system consisted of a mixture of water with 0.1% TFA (solvent A) and CH_3CN with 0.1% trifluoroacetic acid (TFA) (solvent B), using the following gradient: 0–5 min, 5 → 30% A; 5–7 min 30% A; 7–10 min 5% A at a flow rate of 1.3 mL/min.

2.1.2. Radiosynthesis

Radiosynthesis of [^{18}F]MEL050 was performed on an AllInOne™ synthesis module using an in-house reaction sequence (Fig. 1) described in Table 1. The list of reagents and materials used in the automated procedure is presented in Table 2.

[^{18}F]MEL050 was synthesized using one-step bromine-for-fluorine nucleophilic heteroaromatic substitution, inspired by previous publications [21–23].

The aqueous [^{18}F]fluoride target solution was loaded on a QMA (Preconditioned Sep.-Pak® Light QMA cartridge, ABX). The concentrated [^{18}F]fluoride was eluted into the reactor using a K_2CO_3 (3 mg) and Kryptofix (K222, 15 mg) mixed solution (1 mL, CH_3CN/H_2O, 80:20, *v*/v). The solvents were evaporated under reduced pressure at 110 °C for 7 min. To the dry residue containing the K222/potassium [^{18}F]fluoride complex was added the bromo precursor (2 mg) in DMF (1 mL) and the mixture was heated and maintained at 150 °C for 6 min. After cooling, the HPLC mobile phase (2.5 mL) was added to the reaction mixture. The resulting solution was injected onto semi-preparative HPLC system. The fraction containing [^{18}F]MEL050, associated to a well-defined radioactive peak was collected at 10–12 min. The collected fraction was diluted with 20 mL of water, and the resulting solution passed through a C18 cartridge (Sep-Pak® Plus C18 environmental, Waters). The cartridge with radioactive product retained was washed with water (10 mL) before being eluted with 1 mL of ethanol and then 10 mL of saline. The radiotracer solution was finally passed through a 0.22 μm Millipore filter into a sterile vial for *in vivo* experiments.

2.1.3. Quality control

The radiochemical and chemical purity, stability and specific activity measurements were performed by analytical HPLC. The specific activity of the radiotracer was assessed by measurement of the radioactivity injected and the MEL050 concentration in the sample, derived from the UV detection.

The identity of the labeled compound [^{18}F]MEL050 was confirmed by co-injection with a non-radioactive standard of MEL050. The MEL050 concentration in the radioactive sample was obtained using

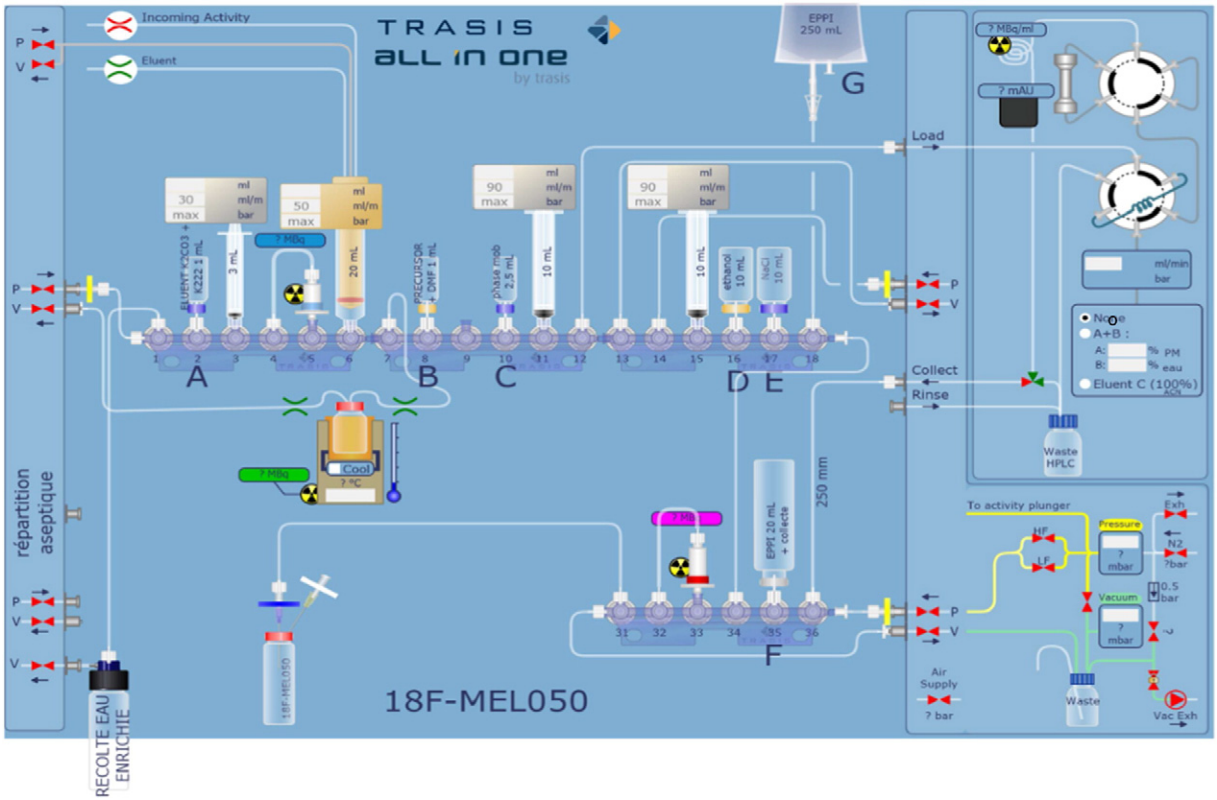

Fig. 1. User interface of AllinOne™ adapted for radiosynthesis of [^{18}F]MEL050.

the UV-peak area ratio between the radioactive product and the standard solution.

2.2. Other radiotracers

[^{18}F]FDG (Flucis®) was graciously supplied free of charge by IBA CIS bio international (France).

2.3. Cell cultures

The B16-F10-luc2 cells (murine melanoma cells, Caliper life sciences, USA) were kindly provided by Dr. Marie Dutreix (Institut Curie, France). Cell cultures were maintained as monolayers in RPMI 1640 (Gibco, Cergy Pontoise, France) medium containing 10% heat-inactivated Fetal Bovine Serum (Gibco) and antibiotics (100 mg/mL streptomycin and 100 mg/mL penicillin; Gibco). The cells were grown at 37 °C in a humidified incubator containing 5% CO2.

Table 1
Reaction sequence for [^{18}F]MEL050 radiosynthesis.

Fluorination of bromo-precursor
1. [^{18}F]fluoride trapping on a pre-activated QMA cartridge
2. [^{18}F]fluoride desorption by eluent
3. Azeotropic evaporation at 110 °C for 7 min
4. Addition of bromo-precursor to the reactor vial
5. [^{18}F]fluorination at 150 °C for 6 min
6. Cooling the reactor vial
7. Addition of HPLC mobile phase to the reactor vial
Purification of [^{18}F]MEL050
1. Injection on HPLC preparative
2. Collection of [^{18}F]MEL050
Formulation of [^{18}F]MEL050
1. Dilution of the collected fraction with water
2. Formulation on a C18 cartridge
3. Sterile filtration

2.4. Animal models

All animal experiments were performed in accordance with European guidelines for care of laboratory animals (2010/63/EU) and were approved by the Animal Ethics Committee of Paris Nord.

In vivo quality control of [^{18}F]MEL050 (biodistribution studies) was performed in 7 weeks-old NMRI (nu/nu) mice (Janvier, France) (n = 4).

For primary subcutaneous tumor models, 10^6 B16-F10-luc2 cells in 100 μL of culture serum-free medium were inoculated by subcutaneous injection on the right flank of 7 weeks old NMRI (nu/nu) mice (n = 4).

For experimental metastatic models, $0.5x10^6$ B16-F10-luc2 cells in 100 μL of PBS were injected into the lateral tail vein of 7 weeks old NMRI (nu/nu) mice (n = 4).

All animals underwent 3 *in vivo* imaging procedures: bioluminescence imaging on day12 after tumor cells inoculation, PET/CT using [^{18}F]MEL050 on day12, then PET/CT using [^{18}F]FDG on day14. Then the animals were sacrificed, tumors were excised for *ex-vivo* volume measurement.

2.5. In vivo bioluminescence imaging

On the twelfth day after tumor induction, bioluminescence imaging was performed using the IVIS Spectrum imaging system (Perkin Elmer)(n = 8). The images were acquired 15 min after i.p. injection of luciferin (15 mg/mL, 0.2 mL) and anesthesia was induced with isoflurane/oxygen, 2.5%. Then the mice were placed in the IVIS chamber for imaging. Anesthesia was continued during the procedure with 2% isoflurane/oxygen introduced *via* a nose cone. Planar anterior and right profil images were acquired with 300 s exposure time.

2.6. In vivo PET/CT imaging

PET/CT imaging was performed using Inveon PET/CT scanner (Siemens Medical Solutions) designed for small laboratory animals.

Table 2
Reagents and materials for the AllinOne™ synthesis module for [^{18}F]MEL050 radiosynthesis.

Entry	Position	Reagents or materials	Quantities
1	5	Pre-conditioned Sep.-Pak® Light QMA	1
2	2 (vial A)	Eluent QMA (solution of K_2CO_3/K222 in CH_3CN/H_2O, 80:20, *v*/v)	1 mL
3	8 (vial B)	Precursor in DMF	2 mg in 1 mL
4	10 (vial C)	Mobile phase	2.5 mL
5	35 (vial F)	Collected fraction vial	1
6	18 (bag G)	EPPI	20 mL + 10 mL
7	33	Sep-Pak® Plus C18 environmental	1
8	16 (vial D)	Ethanol	1 mL
9	17 (vial E)	Saline	10 mL
10		0.22 μm sterile filter	1

Mice were anesthetized (isoflurane/oxygen, 2.5% for induction at 0.8–1.5 L/min and 1.5% at 0.4–0.8 L/min thereafter) during injection of [^{18}F]MEL050 (9.9+/− 1.5 MBq) or [^{18}F]FDG (11.3+/− 1.3 MBq) in a volume of 0.15 mL *via* the tail vein, and during PET/CT acquisitions. Then mice were placed in the PET camera in prone position under isoflurane anesthesia and respiratory monitoring.

For [^{18}F]MEL050 biodistribution studies in control mice, dynamic listmode PET acquisitions were performed from time of radiotracer injection until 90 min after injection (n = 4). The dynamic listmode contains fifteen frames (5 × 60 seconds, 3 × 300 seconds, 7 × 600 seconds).

For PET/CT imaging in primary subcutaneous tumor and pulmonary metastases models, mice were kept in standby for 1 h after radiotracer injection, then were re-anesthetized for a 20 min-duration static PET acquisition followed by a 10 min-duration CT acquisition for attenuation correction of PET images and anatomic localization of PET signals, as the methodology described by Denoyer et al. [22].

The spatial resolution of Inveon PET device was 1.4 mm full-width at half-maximum (FWHM) at the centre of the field of view (FOV). Images were reconstructed using a 2-D ordered subset expectation maximization (Fourier rebinning/2-D OSEM) method including corrections for scanner dead time, scatter radiations and randoms.

2.7. Data analysis

Bioluminescence and PET/CT images were visually assessed.

Then quantitative analysis of PET/CT images was performed by drawing volumes of interest in organs for biodistribution studies, and involving whole volume of visible tumors for quantification of radiotracers' tumor uptake.

To compare static acquisition images, all values of radioactivity concentrations were normalized by the injected dose and expressed as percentage of the injected dose per g of tissue (% ID/g). These % ID/g, both in tumors and thigh muscles, were obtained from the volumes of interest drawn on 20 min duration static acquisition images performed 1 h after injection. The software calculates % ID/g in each voxel of the volume of interest drawn on the images. Then the Tumor-to-Background-Ratio (TBR) was calculated as max % ID/g in tumor divided by max % ID/g in muscles. The max %ID/g value obtained in the volume of interest (in each 20 min duration static acquisition image) was considered for quantitative analysis as performed with standardized uptake value (SUV) in patients.

2.8. Statistical analysis

Data are presented as mean ± SD.

Statistical analysis was performed using JMP, version 5.0.1.2 of SAS® (SAS institute Inc., Cary, NC, USA). A non-parametric statistical hypothesis test (Wilcoxon signed-rank test) was used when two groups of data were compared ([^{18}F]MEL050 *vs* [^{18}F]FDG uptake in tumors on PET/CT). A significance value of $p < 0.05$ was used.

3. Results

3.1. Automated radiosynthesis and characterization of [^{18}F]MEL050

Successful implementation of radiosynthesis of [^{18}F]MEL050 using the AllInOne™ module, including HPLC purification and formulation, was implemented to obtain an overall radiosynthesis time of 48 min, with an end-of-synthesis yield of 13–18 (not decay corrected). [^{18}F]MEL050 was obtained from 2 mg of the bromo-precursor. The fluorination step included heating at 150 °C for 6 min. In-house reaction sequence was designed and used with a dedicated configuration of reaction manifold assembled in-house from individual components provided in vrac by TRASIS (Fig. 1, Tables 1 and 2). HPLC purification was optimized to obtain a clear preparative HPLC separation of [^{18}F]MEL050 from unreacted [^{18}F]fluoride and precursor (Waters Symmetry® Semi-Prep C18 column (300 × 7.8 mm, 7 μm) ; mobile phase: acetonitrile/20 mM ammonium bicarbonate [NH4HCO3] (20:80, *v*/v); flow rate of 3.0 mL/min). In these isocratic semi-preparative HPLC conditions, the [^{18}F]MEL050 is collected at 10–12 min. The efficient separation of [^{18}F]MEL050 from other compounds is shown in Fig. 2.

Taking into account the HPLC mobile phase composition, a formulation step was implemented and automatized using C18 cartridge (Sep-Pak® Plus C18 environmental, Waters) aiming to eliminate the mobile phase and concentrate the radiotracer. The cartridge reformulation procedure is considered advantageous in comparison with solvent evaporation used elsewhere; it contributed to reduce total production time and improve reproducibility of the method, making it more convenient for routine production of the radiopharmaceutic compounds.

Finally, the radiotracer was produced in radiochemical purity of >99%, as confirmed by analytical HPLC (Fig. 3). For all batches produced, the activity concentration of product obtained varied within the range of 0.91–1.95 GBq/mL. The specific activity was within the range of 177–325 GBq/μmol and the radiochemical purity was maintained at >98% over 6 h in saline.

3.2. Biodistribution

Visual analysis demonstrated physiologic [^{18}F]MEL050 uptake in retina, thyroid, stomach, biliary and renal excretion. Quantification of tracer uptake in organs from time of injection to 90 min post-injection is reported in Table 3.

3.3. Tumor involvement

Excision of primary subcutaneous tumors after sacrifice demonstrated several subcutaneous black tumor nodules at the site of tumor cells injection but also distantly (local spreading) in all 4 mice, of 1 mm to 15 mm larger diameter. Multiple infra-millimetric black tumors disseminated in the 2 lungs were found in all mice injected intravenously with tumor cells.

3.4. Bioluminescence imaging

All mice injected subcutaneously with tumor cells (n = 4) were positive in the right flank regarding the primary subcutaneous tumor. All mice injected intravenously with tumor cells were positive in the lungs (Figs. 4 and 5).

3.5. PET/CT imaging

On visual analysis, [^{18}F]MEL050 PET/CT was concordant with bioluminescence imaging, showing increased radiotracer uptake in all subcutaneous tumors and in pulmonary metastases of all mice injected intravenously with tumor cells. The sensitivity of [^{18}F]MEL050 PET/CT images was very high: infra-millimetric lesions were clearly seen

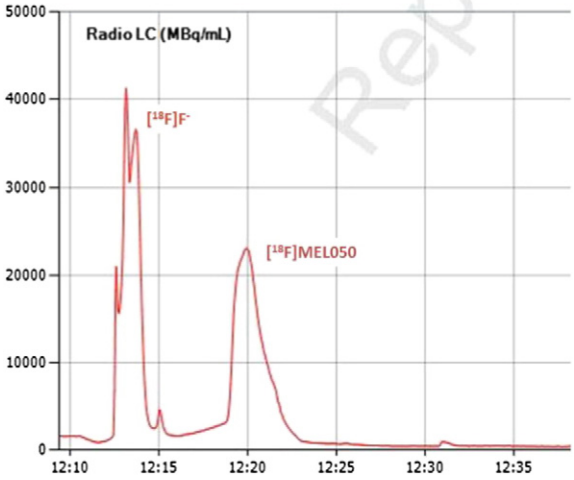

Fig. 2. Typical semi-preparative HPLC radiochromatogram of [^{18}F]MEL050 purification. The relative intensity of the radioactive signal is expressed as MBq/mL. Retention time of the radiotracer is between 10 and 12 min. Conditions: semi-preparative column C18 (Waters Symmetry® Semi-Prep C18 column, 300 × 7.8 mm, 7 μm); solvents: CH_3CN in 20 mM aqueous solution of NH_4HCO_3 (20:80, *v*/*v*); flow rate: 3.0 mL/min.

(Figs. 4 and 5), including small subcutaneous secondary nodules next to primary tumors (Fig. 5).

[^{18}F]FDG PET/CT was positive in all subcutaneous tumors >1 mm, and negative in all pulmonary metastases.

PET quantification of radiotracers uptake in tumors and muscles (max %ID/g) demonstrated higher Tumor-to-Background-Ratio (TBR: max %ID/g in tumors / max %ID/g in muscles) with [^{18}F]MEL050 than with [^{18}F]FDG in pulmonary metastases (10.71 ± 6.57 *vs* 2.67 ± 2.75, p = 0.0059) (Fig. 6a), and similar TBR with [^{18}F]MEL050 and [^{18}F]FDG in subcutaneous tumors (18.59 ± 6.73 *vs* 17.08 ± 6.76, NS) (Fig. 6b).

4. Discussion

The first aim of our work was to implement a fully automated radiosynthesis of [^{18}F]MEL050, including HPLC purification and formulation, using, for the first time, the AllInOne™ synthesis module. In this project the new radiosynthesizer demonstrated perfectly satisfactory capabilities in terms of number of reactors, valves, reagent vial positions, purification capabilities, and reaction temperatures and pressures ranges.

The radiosynthesis scheme and architecture are derived from that described by Greguric et al. [22], except that we opted for the use of the bromo-precursor, already explored once by Rbah-Vidal et al. [21], instead of the chloro-precursor used in other publications. The rationale for this replacement is an expected improvement in radioactive fluorine incorporation (up to 79 *vs* 50%, reported by Rbah-vidal et al. [21], when using a bromo-precursor), a better HPLC separation of the non-consumed precursor from the final product, and hopefully improved chemical purity of the precursor in terms of presence of carrier fluorine, hence improvement of the specific activity of the final product.

This modification justified a reduction of precursor quantity in comparison with that suggested for the chloro-precursor (2 mg instead of 5 mg) [23]. This change was also encouraged by the recent demonstration by Pascali et al. [24] that higher precursor concentrations are not necessary to obtain higher incorporation yields, whereas lower quantities conduct indeed to their reduction.

Finally, introduction of the cartridge formulation of the final product allowed us to avoid the solvent evaporation step, as previously described [21].

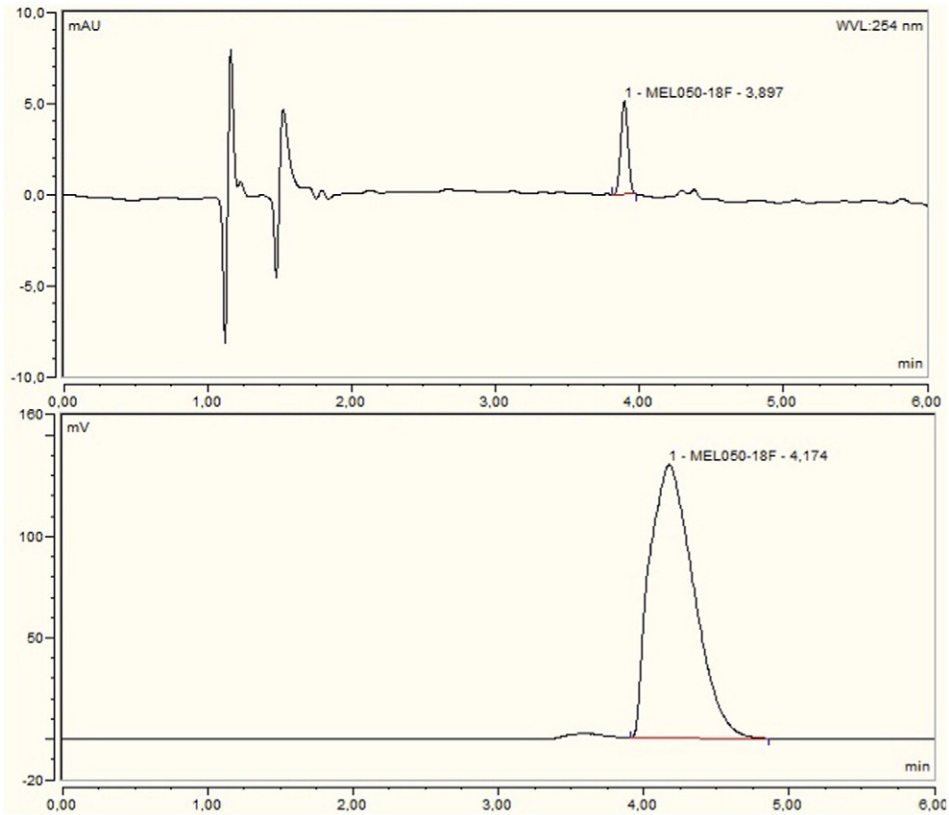

Fig. 3. Analytical HPLC radiochromatogram of [^{18}F]MEL050 (UV 254 nm on the top and radioactivity on the bottom) Retention time of the radiotracer is 4.0 min. Conditions: analytical column C18 (Waters Symmetry® C18 column, 150 × 4.6 mm, 5 μm); solvents: water with 0.1% TFA (solvent A) and CH_3CN with 0.1% TFA (solvent B); gradient system: 0–5 min, 5- > 30% A; 5–7 min 30% A; 7–10 min 5% A; flow rate: 1.3 mL/min.

Table 3
PET biodistribution of [^{18}F]MEL050 (%ID/g of tissue; n = 4).

Time after IV injection (min)						
Organ	1–2	4–5	10–15	30–40	60–70	80–90
Eye	3.19 ± 0.90	3.16 ± 0.78	2.41 ± 0.43	1.56 ± 0.20	0.92 ± 0.12	0.69 ± 0.10
Liver	12.02 ± 1.91	9.28 ± 1.38	5.95 ± 0.79	3.44 ± 0.33	2.26 ± 0.24	1.78 ± 0.19
Heart	3.99 ± 0.47	2.62 ± 0.28	1.82 ± 0.18	1.10 ± 0.15	0.71 ± 0.11	0.57 ± 0.11
Lung	4.20 ± 0.89	2.98 ± 0.74	1.87 ± 0.47	1.00 ± 0.22	0.66 ± 0.15	0.52 ± 0.11
Bone	3.05 ± 0.42	3.05 ± 0.26	2.94 ± 0.18	2.58 ± 0.17	2.31 ± 0.22	2.18 ± 0.22
Kidneys	48.67 ± 28.97	30.32 ± 16.56	14.58 ± 6.74	9.79 ± 5.07	4.16 ± 1.54	2.97 ± 0.96
Thyroid	3.65 ± 0.46	4.93 ± 0.52	6.56 ± 0.73	7.19 ± 0.86	6.48 ± 0.84	5.68 ± 0.79
Muscle	1.47 ± 0.44	1.61 ± 0.38	1.53 ± 0.31	1.18 ± 0.17	0.92 ± 0.12	0.76 ± 0.10
Brain	1.89 ± 0.86	2.04 ± 0.70	2.07 ± 0.51	1.79 ± 0.40	1.38 ± 0.40	1.17 ± 0.40

[^{18}F]MEL050 was produced with satisfactory radiochemical yields and high radiochemical and chemical purity (>99%). The final specific activity obtained in this work (177–325 GBq/μmol) with only 2 mg of bromo-precursor was higher than that previously obtained with 5 mg of the same bromo-precursor (70–80 GBq/μmol [21]), and comparable to that obtained with 5 mg of the chloro-precursor (240–325 GBq/μmol [23]). Variation of chemical purity of the precursors used by the different cited teams is a probable explanation for such differences.

In summary, the procedure proposed offers advantages in terms of facility and organization, combining the efficient HPLC purification of the final product due to the bromo-precursor used, and to the elimination of the solvent evaporation step, replaced by the cartridge reformulation procedure. One should note that no significant improvement in terms of yield or specific activity was observed that could be attributed to use of the bromo-precursor.

The final product displayed necessary radiochemical stability in physiological saline with no stabilizing additives, the radiochemical purity being maintained at >98% over 6 h.

For a practical example, from an irradiated target of 101 GBq recovered on the QMA cartridge of AllinOne™, 15.5 GBq of final formulated product were obtained in 12 mL of injectable solution with activity concentration of 1.3 GBq/mL, and radiotracer specific activity of 229 GBq/μmol.

The limited total production time of [^{18}F]MEL050, less than 50 min, including purification and formulation, makes the radiotracer and the procedure developed easily adaptable for routine production.

The *in vivo* validation of the radiotracer was obtained by PET imaging in control mice to verify *in vivo* stability and normal biodistribution, and in mice bearing pigmented melanomas to verify specific accumulation in tumors with higher sensitivity of detection than [^{18}F]FDG, as previously reported [19].

Our *in vivo* evaluation of [^{18}F]MEL050 as well as the comparison of [^{18}F]MEL050 and [^{18}F]FDG in primary and metastatic melanoma has been performed by experimental approaches similar to the procedure described by Denoyer et al. [19] but using other mice models. Our results confirm those previously reported data.

The luciferase-transfected murin model that we have used allowed us to compare luminescence image and PET imaging in the same animals and to confirm better sensitivity and spatial resolution for PET in both s/c and pulmonary tumor (Figs. 5 and 6).

PET/CT imaging demonstrated *in vivo* stability of the radiotracer and confirmed biodistribution characteristics comparable to those previously reported in mice except that lower radiotracer uptake was observed in the retina. This may be due to the fact that we used white NMRI and not C57BL/6 mouse strain used in other studies [15,20–22,25–27], since [^{18}F]MEL050 uptake in cells is related to pigmentation [28]. PET/

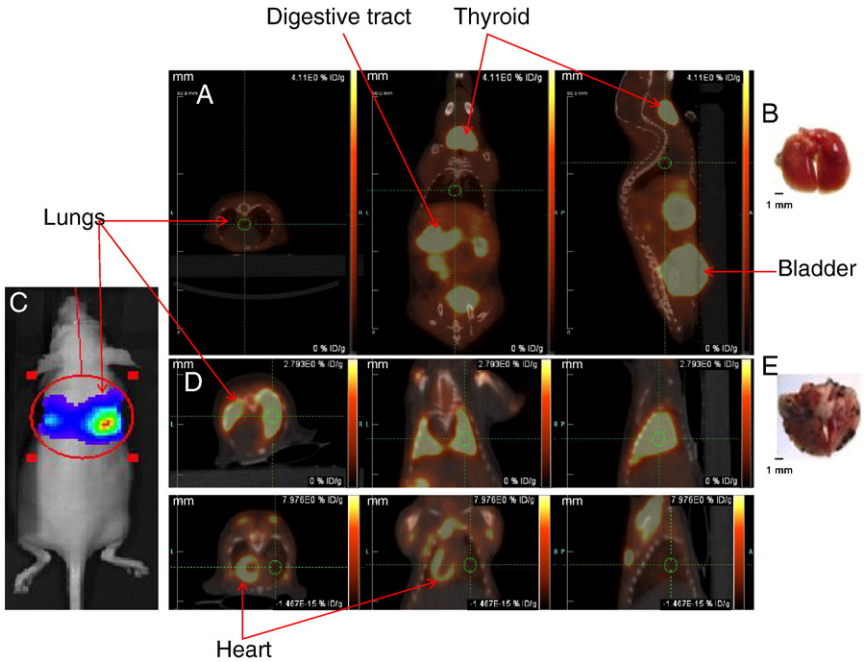

Fig. 4. *In vivo* imaging and photographs of normal and pulmonary metastases. 4 A,B: [^{18}F]MEL050 PET/CT (4A) and extracted lungs (4B) of a control mouse; 4C,D,E: Bioluminescence imaging (4C), corresponding [^{18}F]MEL050 (top) and [^{18}F]FDG (bottom) PET/CT images (4D), and extracted lungs (4E) of a mouse with pulmonary metastases. Fluorescence and high [^{18}F]MEL050 uptake are observed in the lungs invaded by small sub-millimetric black tumors (melanoma B16-luciferine expressing cells), whereas no [^{18}F]FDG uptake is observed in the lungs of the same mouse.

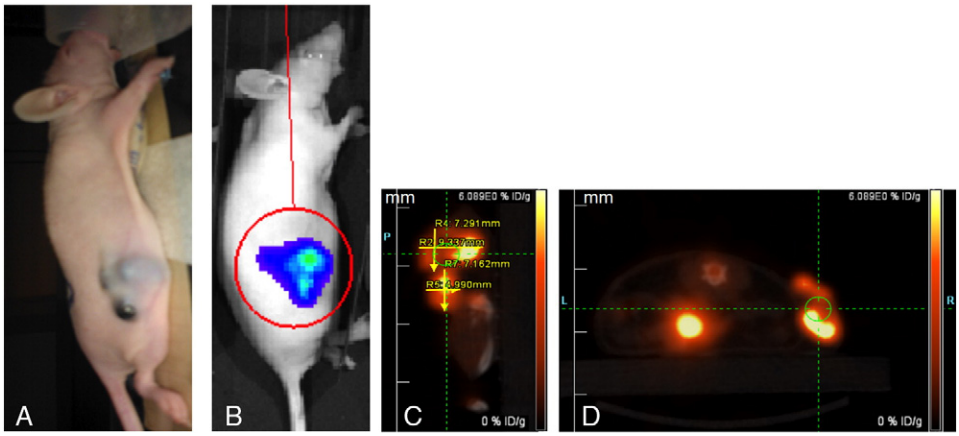

Fig. 5. Photograph, bioluminescence and [^{18}F]MEL050 PET/CT imaging of a mouse with primary subcutaneous melanoma. 5A: photograph showing 3 subcutaneous black tumors in the right flank; 5B: corresponding bioluminescence imaging (luciferine expressing B16 cells) of the tumors; 5C: corresponding sagittal [^{18}F]MEL050 PET/CT images; 5D: corresponding axial [^{18}F]MEL050 PET/CT images.

CT imaging in mice with pigmented melanoma confirmed better detection of sub-millimetric tumors with [^{18}F]MEL050 than with [^{18}F]-FDG, with a very high Tumor-to-Background-Ratio (>10), as previously reported [21]. This was particularly significant in the pulmonary metastases model, in which all [^{18}F]-FDG PET/CT images were negative.

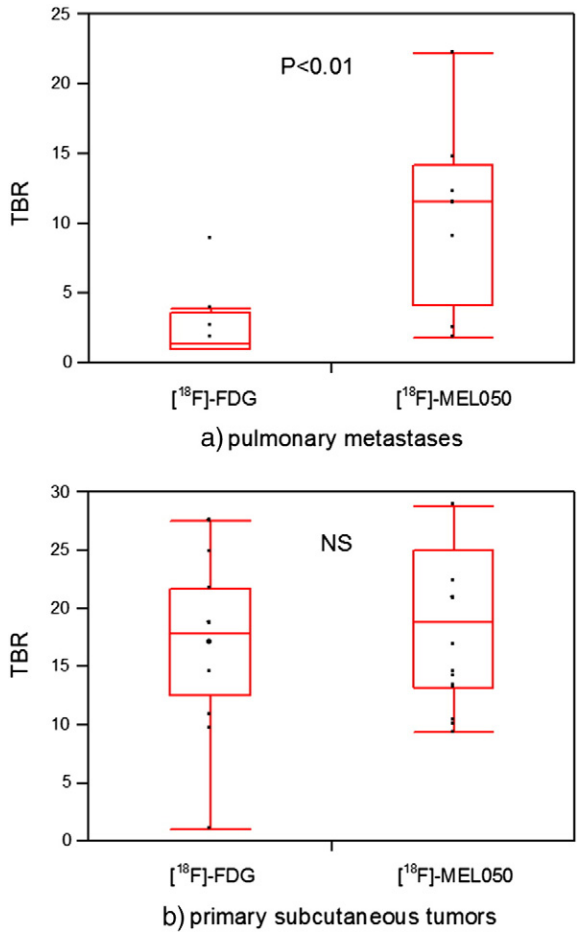

Fig. 6. PET quantification of [^{18}F]MEL050 and [^{18}F]FDG in pulmonary metastases (a) and in primary subcutaneous tumors (b).

5. Conclusion

In summary, we have demonstrated that the fully automated synthesis of [^{18}F]MEL050, including HPLC purification and formulation, can be easily performed on the AllinOne™ radiosynthesizer. This fully automated synthesis provides the [^{18}F]MEL050 with high radiochemical purity and substantial specific activity in a limited time.

The ability of [^{18}F]MEL050 to detect small melanoma lesions is demonstrated by our data, in both primary subcutaneous tumors and pulmonary metastases (which were all inframillimetric). Therefore as a conclusion, we enhanced the potential of this tracer to allow detection of very small lesions in patients, ie at a very early stage of the disease. In addition, we showed higher specific [^{18}F]MEL050 uptake in sub-millimetric pulmonary metastases, comparatively to [^{18}F]FDG.

References

[1] Jemal A, Siegel R, Ward E, Hao Y, Xu J, Thun MJ. Cancer statistics. Cancer J Clin 2009; 59:225–49.
[2] National Cancer Institute, surveillance, epidemiology, and end results program. http://seer.cancer.gov/statfacts/html/melan.html. [accessed 08.05.16].
[3] Nikolaou V, Stratigos AJ. Emerging trends in the epidemiology of melanoma. Br J Dermatol 2014;170:11–9.
[4] Institut national du cancer (INCa), rapport 1018 - incidence projetée en 2015 du mélanome cutané. http://lesdonnees.e-cancer.fr/les-fiches-de-synthese/1-types-cancer/14-melanome-cutane/50-incidence-france-melanome-cutane.html. [accessed 08.05.16].
[5] Jemal A, Siegel R, Ward E, Hao Y, Xu J, Murray T, et al. Cancer statistics. Cancer J Clin 2008;58:71–96.
[6] Mouawad R, Sebert M, Michels J, Bloch J, Spano JP, Khayat D. Treatment for metastatic malignant melanoma: old drugs and new strategies. Crit Rev Oncol Hematol 2010;74:27–39.
[7] Gibney GT, Messina JL, Fedorenko IV, Sondak VK, Smalley KS. Paradoxical oncogenesis–the long-term effects of BRAF inhibition in melanoma. Nat Rev Clin Oncol 2013;10:390–9.
[8] Della Vittoria Scarpati G, Fusciello C, Perri F, Sabbatino F, Ferrone S, Carlomagno C, et al. Ipilimumab in the treatment of metastatic melanoma: management of adverse events. Onco Targets Ther 2014;7:203–9.
[9] Boyle GM. Therapy for metastatic melanoma: an overview and update. Expert Rev Anticancer Ther 2011;11:725–37.
[10] Ross MI. Sentinel node biopsy for melanoma: an update after two decades of experience. Semin Cutan Med Surg 2010;29:238–48.
[11] Schüle SC, Eigentler TK, Garbe C, La Fougère C, Nikolaou K, Pfannenberg C. Influence of (18)F-FDG PET/CT on therapy management in patients with stage III/IV malignant melanoma. Eur J Nucl Med Mol Imaging 2016;43:482–8.
[12] Eisenhut M, Hull WE, Mohammed A, Mier W, Lay D, Just W, et al. Radioiodinated N-(2-diethylaminoethyl)benzamide derivatives with high melanoma uptake: structure-affinity relationships, metabolic fate, and intracellular localization. J Med Chem 2000;43:3913–22.
[13] Chezal JM, Papon J, Labarre P, Lartigue C, Galmier MJ, Decombat C, et al. Evaluation of radiolabeled (hetero)aromatic analogues of N-(2-diethylaminoethyl)-4-iodobenzamide for imaging and targeted radionuclide therapy of melanoma. J Med Chem 2008;51:3133–44.

[14] Oltmanns D, Eisenhut M, Mier W, Haberkorn U. Benzamides as melanotropic carriers for radioisotopes, metals, cytotoxic agents and as enzyme inhibitors. Curr Med Chem 2009;16:2086–94.
[15] Maisonial A, Kuhnast B, Papon J, Boisgard R, Bayle M, Vidal A, et al. Single photon emission computed tomography/positron emission tomography imaging and targeted radionuclide therapy of melanoma: new multimodal fluorinated and iodinated radiotracers. J Med Chem 2011;54:2745–66.
[16] Bacin F, Michelot J, Bonafous J, Veyre A, Moreau MF, Kemeny JL, et al. Clinical study of [123I]N-(2-diethylaminoethyl)-4-iodobenzamide in the diagnosis of primary and metastatic ocular melanoma. Acta Ophthalmol Scand 1998;76:56–61.
[17] Sillaire-Houtmann I, Bonafous J, Veyre A, Mestas D, D'Incan M, Moins N, et al. Phase 2 clinical study of 123I-N-(2-diethylaminoethyl)-2-iodobenzamide in the diagnostic of primary and metastatic ocular melanoma. 2004;27:34–9.
[18] Cachin F, Miot-Noirault E, Gillet B, Isnardi V, Labeille B, Payoux P, et al. 123I-BZA2 as a melanin-targeted radiotracer for the identification of melanoma metastases: results and perspectives of a multicenter phase III clinical trial. J Nucl Med 2014;55:15–22.
[19] Denoyer D, Greguric I, Roselt P, Neels OC, Aide N, Taylor SR, et al. High-contrast PET of melanoma using 18F-MEL050, a selective probe for melanin with predominantly renal clearance. J Nucl Med 2010;51:441–7.
[20] Denoyer D, Potdevin T, Roselt P, Neels OC, Kirby L, Greguric I, et al. Improved detection of regional melanoma metastasis using 18F-6-Fluoro-N-[2-(diethylamino)ethyl] pyridine-3-Carboxamide, a melanin-specific PET probe, by Perilesional administration. J Nucl Med 2011;52:115–22.
[21] Rbah-Vidal L, Vidal A, Besse S, Cachin F, Bonnet M, Audin L, et al. Early detection and longitudinal monitoring of experimental primary and disseminated melanoma using [18F]ICF01006, a highly promising melanoma PET tracer. Eur J Nucl Med Mol Imaging 2012;39:1449–61.
[22] Greguric I, Taylor SR, Denoyer D, Ballantyne P, Berghofer P, Roselt P, et al. Discovery of [18F]N-(2-(diethylamino)ethyl)-6-fluoronicotinamide: a melanoma positron emission tomography imaging radiotracer with high tumor to body contrast ratio and rapid renal clearance. J Med Chem 2009;52:5299–302.
[23] Greguric I, Taylor S, Pham T, Wyatt N, Jiang CD, Bourdier T, et al. Radiosynthesis of a novel PET fluoronicotinamide for melanoma tumour PET imaging; [18F]MEL050. Aust J Chem 2011;64:873.
[24] Pascali G, Matesic L, Collier TL, Wyatt N, Fraser BH, Pham TQ, et al. Optimization of nucleophilic 18F radiofluorinations using a microfluidic reaction approach. Nat Protoc 2014;9:2017–29.
[25] Billaud EMF, Rbah-Vidal L, Vidal A, Besse S, Tarrit S, Askienazy S, et al. Synthesis, Radiofluorination, and in vivo evaluation of novel fluorinated and iodinated radiotracers for PET imaging and targeted radionuclide therapy of melanoma. J Med Chem 2013;56:8455–67.
[26] Billaud EMF, Maisonial-Besset A, Rbah-Vidal L, Vidal A, Besse S, Béquignat JB, et al. Synthesis, radiolabeling and preliminary in vivo evaluation of multimodal radiotracers for PET imaging and targeted radionuclide therapy of pigmented melanoma. Eur J Med Chem 2015;92:818–38.
[27] Maisonial A, Billaud EMF, Besse S, Rbah-Vidal L, Papon J, Audin L, et al. Synthesis, radioiodination and in vivo screening of novel potent iodinated and fluorinated radiotracers as melanoma imaging and therapeutic probes. Eur J Med Chem 2013;63:840–53.
[28] Mansard S, Papon J, Moreau MF, Miot-Noirault E, Labarre P, Bayle M, et al. Uptake in melanoma cells of N-(2-diethylaminoethyl)-2-iodobenzamide (BZA2), an imaging agent for melanoma staging: relation to pigmentation. Nucl Med Biol 2005;32:451–8.